PCCP

Accepted Manuscript

ROYAL SOCIETY OF CHEMISTRY

www.rsc.org/pccp

Anisotropic structure and dynamics of the solvation shell of a benzene solute in liquid water from *ab initio* molecular dynamics simulations

Ashu Choudhary and Amalendu Chandra

Department of Chemistry, Indian Institute of Technology Kanpur, India 208016

Abstract

The anisotropic structure and dynamics of the hydration shell of a benzene solute in liquid water have been investigated by means of *ab initio* molecular dynamics simulations using the BLYP (Becke-Lee-Yang-Parr) and the dispersion corrected BLYP-D functionals. The main focus has been to look at the influence of π-hydrogen-bonding and hydrophobic interactions on the distance and angle resolved various structural and dynamical properties of solvation shell. The structure of hydration shell water molecules around benzene are found to be highly anisotropic as revealed by the radial distribution functions of different conical regions and joint radial/angular distribution functions. The benzene-water dimer potential energy curves are calculated for a variety of orientation of water along the axial and equatorial directions for both BLYP and BLYP-D functionals. The simulation results of the hydration shell structure of benzene, particularly the axial and equatorial benzene-water RDFs are discussed based on the differences in the benzene-water potential energies for different orientations and functionals. The inter-particle distance/angle correlations show an enhanced water structure in the solvation shell of benzene compared to that between the solvation shell and bulk and also between the bulk molecules. On average, a single πH-bond is found to be formed between water and benzene in the 45° axial conical region of the solvation shell. The πH-bonded water molecules are found to have faster translational dynamics and also found to follow a fast jump mechanism of reorientation to change their hydrogen bonded partners. The presence of π-hydrogen-bonded water makes the overall dynamics of the axial region faster than that of the equatorial region where the water molecules are hydrophobically solvated and hydrogen bonded to other water molecules.

1 Introduction

Aromatic hydrocarbons are important building blocks for many biological molecules and hydrophobic surfaces[1–5]. Therefore, studies of hydration of aromatic hydrocarbons are important as water is the omnipresent solvent for biological systems. The aromatic hydrocarbons differ from the aliphatic ones by the cyclic ring structures with delocalized π-electrons. The interaction of π-electrons of aromatic hydrocarbons with water hydrogen is known as π-hydrogen-bonding (πH-bonding)[6]. These πH-bonds are considered to be one of the most important characteristic features of biological interfaces containing aromatic groups. These πH-bonds allow a higher probability of donor displacement and bending of hydrogen bond angle, thus possess a softer geometry compared to other conventional hydrogen bonds[7]. In order to understand the properties of πH-bonded water molecules and also of other water molecules in the solvation shell of aromatic hydrocarbons, the simplest aromatic hydrocarbon molecule of benzene has been used as a model system in various earlier studies[6–24]. Several spectroscopic studies have confirmed the formation of πH-bonds between benzene and water at ambient conditions[6–16]. These studies suggest that approximately one πH-bond is formed between water and benzene in the axial region with respect to the plane of the benzene molecule. A recent spectroscopic study[8] of very dilute benzene-water solution has revealed a narrow πH-bonded OH peak at 3610 cm^{-1}. This is about 50 cm^{-1} red shifted with respect to the dangling (free) OH peak found at around 3660 cm^{-1}. This frequency shift is also similar to the earlier reported πH-bonded OH stretching frequency shift in case of benzene-$(water)_8$ clusters studied by resonant ion-dip infrared spectroscopy[14]. These spectroscopic studies have provided useful information about the strength of πH-bonds. However, a detailed understanding of the effects of such πH-bonds on the hydration shell structure and dynamics needs further studies.

Benzene is an anisotropic molecule. The water molecules in the axial and equatorial regions around benzene in its solvation shell have different structural and orientational arrangements as confirmed by earlier molecular dynamics[17–22] and first principles[21,23,24] simulation studies. Most of these earlier studies focused on the structural arrangement of water around benzene and revealed that benzene possesses an anisotropic solvation shell. Apart from the average structural behavior, the details of translational and rotational dynamics of water molecules in the regions axial and equatorial to the benzene

solute also need to be quantified because these are governing factors in the dynamics of chemical systems with πH-bonds[25–32]. In the present study, we provide a detailed picture of the solvent dynamics along with benzene-water π-hydrogen-bonded and hydrophobic solvation and organization of water molecules around a benzene solute. The important factors that determine the hydration structure around a nonpolar solute are the directional nature of water hydrogen bonds and tendency of water molecules to adapt suitable structural configurations to maximize the number of hydrogen bonds with neighboring water molecules[2,5,19]. Therefore, our focus in the present study has been to explore the interplay between benzene-water interaction, especially the benzene-water πH-bonding, and water-water hydrogen bonding interactions which govern the subtle changes in the structure and dynamics of the solvation shell around a benzene solute molecule by means of *ab initio* simulations[33,34] without using any empirical potential models. We have looked at the influence of πH-bonding and hydrophobic interactions on the distance and angle resolved structure and dynamics of solvation shell water molecules. Additionally, we have also looked at the possible roles of angular jumps in the reorientational motion of πH-bonded water molecules. For hydrophobic solvation, the so called "iceberg model"[35] predicts an enhanced ordering of the solvation water around small hydrophobic solutes. However, it is still a debatable and controversial issue in the literature. The recent experimental results of slow dynamics of the fraction of solvation water around hydrophobes seem to suggest an enhanced structuring and increased strength of hydrogen bonds[36]. In the current work, we have also looked at this aspect of changes in water-water hydrogen bonded correlations induced by the hydrophobic solute through calculations of inter-particle distance/angle correlations between water molecules in the solvation shell and also in the bulk phase.

In order to adequately capture the essential characteristics of the solvation shell structure and dynamics around benzene, we have performed first principles dynamical simulations[33,34] where the many-body interactions and forces are calculated on-the-fly through quantum electronic structure calculations within density functional theory[37]. We note that such first principles dynamical simulations of benzene-water systems were also carried out in earlier studies[23,24]. However, the current study looks at a rather large set of structural and dynamical properties and also the effects of dispersion corrections on these properties which were not considered in the earlier *ab initio* simulation studies of benzene in water. For example, to the best of our knowledge, the structural properties like

radial/angular distributions, water-water inter-particle distance/angle distributions and hydrogen bonding state distributions discussed later in Section 3 and all the dynamical properties presented in Section 4 and the effects of dispersion corrections on all these structural and dynamical properties are investigated here for the first time for benzene-water system through *ab initio* molecular dynamics simulations. The radial distribution functions of conical regions (Section 3) are also investigated here with better angular resolution than that of earlier *ab initio* simulation studies[23,24]. Additionally, we have also calculated the benzene-water dimer potential energy curves through quantum chemical calculations for a variety of orientations of water along the axial and equatorial directions for both BLYP and BLYP-D functionals. The *ab initio* simulation results of the benzene-water radial distribution functions have been discussed based on the benzene-water potential energy differences for different orientations and density functionals.

We have organized the rest of the paper as follows. In Section 2, we have described the methodology and also other details of simulations. The results of radial distribution functions (RDFs), benzene-water dimer potential energy curves, radial/angular distribution functions and water-water inter-particle distance/angle distributions around a benzene solute in various axial and equatorial conical regions of the solvation shell are presented in Section 3. Section 4 deals with a detailed study of the dynamics of water molecules in different conical regions around benzene and also of the mechanism of π-hydrogen bond reorientation. The results of frequency distributions and frequency time correlation functions are discussed in Section 5. Finally, our conclusions are briefly summarized in Section 6.

2 Simulation Details

The simulations of the current study have been performed by employing the Car-Parrinello method[33,34] and the CPMD code[38]. We have studied a benzene solute dissolved in a liquid of 107 water molecules in a cubic simulation box which is periodically replicated in three dimensions. The edge length of the simulation box is 14.94 Å. The electronic structure of the extended simulation system is represented by the Kohn-Sham (KS) formulation[37] of density functional theory within a plane wave basis. The core electrons are treated via Troullier-Martins[39] pseudo potentials and the plane-wave expansion of the KS

orbitals is truncated at a kinetic energy cut-off of 80 Ry. A fictitious mass of $\mu = 800$ au is assigned to the electronic degrees of freedom. The coupled equations of motion describing the system dynamics are integrated by using a time step of 5 au. The mass of deuterium is assigned to all the hydrogen atoms. We have used the BLYP[40,41] density functional and also the dispersion corrected BLYP-D[42–44] density functional in the present simulations. We note that the BLYP functional was used in many earlier simulations of water[45–57] and aqueous solutions[58–70]. However, many recent studies have shown that inclusion of dispersion corrections[42–44] to generalized gradient approximation (GGA) category functionals such as BLYP provides a better description of water from the perspectives of phase diagram, structure and dynamics[71–79]. Hence, we have employed the dispersion corrected BLYP-D functional also in the current calculations in addition to using the BLYP functional. In particular, we have used the Grimme-D2 version[44] of dispersion correction scheme which uses damped atom-pairwise dispersion corrections of the form $C_6 r^{-6}$ where r represents the distance between two atoms and C_6 is the prefactor that determines the strength of dispersion interaction. In this scheme, three body dispersion interactions are not taken into account. We note that the use of both functionals also allows us to look at the effects of dispersion interactions on the structure and dynamics of the hydration shell of a benzene solute molecule by comparing the results of BLYP and BLYP-D functionals. We also note in this context that the effects of including dispersion by the addition of Grimme-D2 and D3[44,80] in the structure and thermodynamics of liquid water has been discussed extensively by McGrath et al.[72,73]. Further justifications of the use of density functionals and various other simulation parameters are presented in Sections 1-3, Tables S1 and S2 and Fig.S1 of the Supplementary Information[81]. Additionally, we have also performed quantum chemical calculations of the benzene-water dimer potential energies for different orientations of water for both BLYP and BLYP-D functionals using the same 80 Ry cut-off for the plane wave basis as it was done for the simulations, The results of such dimer energy calculations are discussed in the context of our simulated anisotropic structural distributions of benzene-water pairs for both the functionals..

The initial configuration of the system was created through classical molecular dynamics simulation using empirical multi-site potentials[82,83]. After that, we carried out two *ab initio* molecular dynamics simulations using the BLYP and BLYP-D functionals

and equilibrated each system for 20 ps in the canonical ensemble at 298 K and thereafter each run was continued in microcanonical ensemble for another 80 ps for calculations of various equilibrium and dynamical quantities. After the simulated trajectories were generated, the stretch frequencies of OD bonds were calculated by a time series analysis of the respective coordinates and momenta using the wavelet method[84–86]. The details of this time series method for calculations of fluctuating OD bond frequencies from simulation trajectories are available in Refs[47,70]. The results of various calculated structural and dynamical quantities are presented in the following sections. In order to estimate the error bars associated with these calculated averages, we divided the entire production runs of 80 ps into 4 blocks of 20 ps each and calculated the averages for each block. Subsequently, these block averages were used to calculate the standard deviations and percentage error bars of the calculated average values of various quantities.

3 Solvation Structure

We first look at the structure of the solvation shell in order to understand the structural and orientational changes that are induced by a benzene solute on its solvation shell water molecules. We note that in earlier studies[19–21,23,24], specific attention was given to the distinct hydration patterns found in the axial and equatorial regions around benzene at ambient conditions. In the current work, we have further resolved the structural information around a benzene solute molecule by calculating the radial/angular distribution functions and also water-water inter particle distance/angle distributions around the benzene solute, in addition to the benzene-water radial distribution functions (RDFs). We have considered different conical regions around the benzene solute. The regions are as follows: (a) Axial region is defined as the conical region with its axis orthogonal to the benzene ring plane through its centre and angle θ_{axial} of the axial cone is defined as the angle between the principal axis of C_6 symmetry and a vector along the surface of the centre. (b) Equatorial region is defined as the conical region of the solvation shell with its axis in the plane of the benzene ring and the angle θ_{equa} of equatorial cones is defined as the angle between any of in-plane C_2 axis using the benzene center as a reference point and a vector along the surface of the cone. Both the regions are schematically shown in Fig.1 . Both structural and dynamical results discussed in the current work are resolved with respect to these conical shells of different angles so as to capture the

anisotropic nature of the solvation shell from both structural and dynamical perspectives.

3.1 Benzene-Water Radial Distribution Functions and Coordination Numbers

The solvation structure around benzene is characterized by the radial distribution functions (RDFs) for benzene center of mass (Bz)-water oxygen ($g_{Bz-O}(r)$) and also benzene center of mass-water hydrogen ($g_{Bz-D}(r)$) correlations in the axial and equatorial conical regions. Note that the hydrogen atom is represented by D as we have used deuterium mass for H . The $g_{Bz-O}(r)$ and $g_{Bz-D}(r)$ correlations in the axial and equatorial conical regions of 15 °, 30 °, 45 °, 60 °, 75 ° and 90 ° angles are shown in Fig.2 . The RDFs of the 15 ° and 30 ° axial regions show the presence of a sharp first peak for the Bz−O correlations at 3.2 Å and 3.3 Å for the BLYP-D and BLYP functionals, respectively. The corresponding peaks for the Bz−D correlations are found to be located at 2.3 Å and 2.4 Å for the two functionals. The minima for πH-bonding peaks of Bz−O and Bz−D correlations are found to be located at around 3.6 Å and 3.0 Å, respectively, which are the distances corresponding to πH-bonding interaction region of benzene-water system[21]. The heights of the πH-bonding peaks of Bz−O and Bz−D RDFs for the 15 ° and 30 ° axial regions show some difference for the BLYP-D and BLYP functionals. The difference between the BLYP and BLYP-D results is more noticeable for the Bz−D RDFs. The peak height for the 15 ° axial region is maximum for these correlations and the peak height decreases for higher axial conical regions because this π-H-bonding effect gets averaged out in larger axial regions. It shows that the πH-bonding is mainly a feature of the smaller axial conical regions. In the Bz-O RDFs, the second peak starts evolving for larger axial regions and, for the Bz-D RDFs, the position of the already existing second peak also changes with increase in the conical angle of the axial regions. The second peaks correspond to the total solvation shell around the benzene solute. The solvation shell peaks for the Bz−O and Bz−D RDFs shift to larger distances for larger axial regions. The shift of the RDF maximum with larger axial angles indicates that the water molecules are placed far from the benzene center of mass (COM) for larger axial regions which is a signature of the oblate shape of the benzene solvation shell. The RDFs for the BLYP-D functional appear little closer to benzene than that for the BLYP functional. Also, it is interesting to

note that the BLYP-D functional predicts a higher first peak of the Bz-H correlation than the second peak for the smaller conical regions contrary to the predictions of the BLYP functional without any dispersion corrections. Thus, inclusion of dispersion corrections produces a relatively stronger πH-bond compared to that produced by the pure BLYP functional.

The RDFs of the equatorial conical regions are presented in Figs.2(c)-(d) for the Bz-O and Bz-D correlations, respectively. The RDFs of the 15°, 30° and 45° equatorial conical regions start beyond 3.5 Å for Bz−O and 3.0 Å for Bz−D correlations. The oxygen and hydrogen atoms participating in πH-bonding appear in the equatorial regions of angles larger than 45° and, hence, no such small peak corresponding to the πH-bonding region is found in the equatorial regions for the 15°, 30° and 45° conical angles. The first solvation shell peak for different equatorial regions is found to be located at the same position for a particular functional and the peak height is found to decrease for larger equatorial regions. This shows that the water molecules in the smaller equatorial regions are larger in number density and stay farthest from the benzene centre of mass within the solvation shell. In fact, the first solvation shell peak position is primarily determined by the molecular arrangements in the equatorial region. The first solvation shell peak for the BLYP functional is located at a slightly larger distance than that for the BLYP−D functional. It is to be noted that the 90° axial and 90° equatorial cones cover the same region around the benzene solute, *i.e.* the entire first solvation shell.

In Fig.3, we have presented further analysis of different parts of the Bz-O radial distribution functions for the 15^o axial and equatorial conical regions around the benzene solute. Results of both BLYP and BLYP-D functionals are considered. Only the 15^o conical regions are considered because here the objective is to explore the nature of axial and equatorial benzene-water dimeric configurations that contribute to the maxima and minima of benzene-water RDFs in the respective regions. In Fig.3(a), we have shown simulation snapshots of some of the representative benzene-water configurations in the 15^o conical shell at distances of 3.1-3.4 Å and 3.7-3.9 Å from the benzene centre of mass (Bz) that contribute the to the maximum of the 15^o axial RDF. In this figure, we have also shown a representative benzene-water dimer configurations in the 15^o axial conical shell at the distance range of 4.8-6.0 Å from Bz that contributes to the first minimum

of the 15^o axial RDF. Similar simulation snapshots of representative benzene-water configurations are also shown in Fig.3(b) in the 15^o equatorial conical shell at distances of 4.8-5.2 Å and 6.2-7.0 Å from Bz which contribute, respectively, to the maximum and minimum of the 15^o equatorial benzene-water RDF. In Fig.4, we have presented results of our quantum chemical calculations of benzene-water dimer potential energy curves for different orientations of the water molecule in the axial and equatorial directions. The Bz-O distances are kept fixed at 3.4Å and 5.0Å, respectively, in the axial and equatorial directions, while a rotation is given to the water molecule so as to vary its OD orientation with respect to the C_6 of the benzene from -180^o to $+180^o$. Snapshots of dimer configurations are also shown for different parts of the potential energy curves in both axial and equatorial directions. It can be seen that the lowest energy dimer configurations of Fig.4 also contribute to the first maximum of the Bz-O RDFs for both axial and equatorial regions.

The πH-bonding interaction between benzene and water in the axial and equatorial conical regions can be better understood quantitatively through calculations of the coordination numbers. The coordination number corresponding to πH-bonding distance ranges, *i.e.* up to 3.5 Å for Bz-O RDFs and up to 3.0 Å for Bz-D RDFs, are calculated for the axial and equatorial regions around a benzene solute molecule. It is found that altogether ~ 1.2 oxygen atoms and ~ 1.0 hydrogen atom appear in the πH-bonding region. It suggests that on average about one πH-bond is formed between the benzene and water. It is found that in the axial conical region larger than 45°, no change is found in the coordination numbers of oxygen and hydrogen. Hence, the probable region of πH-bond is the axial conical region up to 45°. This is further confirmed by coordination number for the πH-bonding region from the equatorial direction. The 45° axial and 45° equatorial regions can be distinguished in terms of probable πH-bonding and non πH-bonding regions of the benzene solvation shell. Whenever we focus our attention on purely axial or purely equatorial regions, we will be referring to the 45° axial region as the axial and 45° equatorial region as the equatorial region around benzene. In the πH-bonding region, only a slight difference is found in the number of oxygens and hydrogens for the BYLP and BYLP-D functionals. Further details of the πH-bond and coordination numbers for the axial and equatorial conical regions of varying angles are presented in Fig.S2 of the Supplementary Information.

3.2 Benzene-water Radial/Angular Distribution Functions

The orientational preference of water molecules around benzene is studied further by calculating the benzene-water radial/angular distributions[19]. These distributions are calculated for two tilt angles: Water dipole tilt angle ω and the OD bond vector tilt angle α which are defined as the angles that the water dipole and OD vectors make, respectively, with the vector connecting water oxygen to the benzene center of mass ($\vec{r}$). The definitions of these tilt angles are illustrated in Fig.S3 of the Supplementary Information[81]. The plots of the water dipole radial/angular distribution functions $g_{Bz-O}(r, \cos\omega)$ for the axial and equatorial regions are shown in Fig.S4 of the Supplementary Information[81] for the BLYP-D and BLYP functionals. For the 15 ° axial region, the maximum around 3.0 Å which defines the πH-bonded distance range, is found to be around $\cos\omega \approx 0.6$ with the corresponding value of tilt angle $\omega \approx 53$ °. These results are also similar to earlier reported *ab initio* molecular dynamics results for small axial regions[23,24]. On increasing the axial conical regions from 30 ° to 90 °, the distribution of $\cos\omega$ widens. The second peak has two distinct ranges of $\cos\omega$ for the maximum : one from 1.0 to 0.5 and other from -0.5 to -1.0. In case of the BLYP-D functional, for higher axial regions, the stronger peak for the overall solvation shell is found to be around $\cos\omega$ = -0.5 to -1.0, rather than the region of $\cos\omega$ = 1.0 to 0.5 . This shows that for the BLYP-D functional, there is higher probability of water molecules with ω in the range of 120 ° to 180 °. The BLYP functional, on the other hand, predicts almost the same probabilities for ranges of ω from 0 ° to 60 ° and 120 ° to 180 ° for the higher axial regions of the solvation shell. In the equatorial regions, the $\cos\omega$ has its maximum probability around 4.8 Å for both the BLYP and BLYP-D functionals which is consistent with the RDF peaks. The peak for $\cos\omega$ = -0.5 to -1.0 indicates the hydrophobic nature of the benzene solute. The maximum probability region around this maximum is found to be less intense for the BLYP functional which means the hydrophobicity of the benzene ring is captured more strongly by the BLYP-D functional with dispersion corrections. The results and discussions of the radial/angular distributions of the OD tilt angles are presented in Fig.S5 and Sec.5 of the Supplementary Information.

3.3 Water-Water Inter-Particle Distance/Angle Distributions

The inter-particle correlations between water molecules inside the solvation shell and also outside of it are important for better understanding of the solvation shell structure around a hydrophobic solute. In the calculations of these correlations, water molecules having their oxygen atoms within 6.0 Å from benzene centre of mass are taken to be in the first solvation shell (S_1) and the rest are considered as bulk molecules. We calculated the O··O inter-particle distances (R) and the best O··O-D angle (θ), which is the smallest of the four possible angles for each water pair, in different regions. Then, we calculated the water-water inter-particle distance/angle distribution $\rho_{OO}(R,\theta)$[19,87]. The plots of $\rho_{OO}(R,\theta)$ for the solvation shell (Solv-Solv), solvation shell-bulk (Solv-Bulk) and within the bulk (Bulk-Bulk) water molecules are presented in Fig.S6 of the Supplementary Information[81]. The overall shape of $\rho_{OO}(R,\theta)$ is found to be rather similar for the Solv-Solv, Solv-Bulk and Bulk-Bulk water molecules. There are two peaks found for all the cases. The first peak is found to be at R $\approx$ 2.7 Å and $\theta \approx$ 8-10 ° which corresponds to the hydrogen bonded water pairs. The second peak at a larger distance of R $\approx$ 4.2-4.5Å and $\theta \approx$ 40-45 ° corresponds to water pairs that are not hydrogen bonded but in the second contact of each others. The intensity of the first peak is found to be maximum for the water pairs inside the solvation shell. The corresponding peaks for solv-bulk and bulk-bulk pairs have lower relative probability density which shows that the hydrogen bonding interaction within the solvation shell water molecules is enhanced in comparison to solv-bulk or bulk-bulk pairs.

3.4 Hydrogen Bond Distributions

The structure of water around a hydrophobic solute can be better understood by the local arrangement of the hydrogen bonded network. We have used a set of geometric criteria[88–95] for the definition of hydrogen bonds between water-water and benzene-water pairs. A hydrogen bond between two water molecules or between a water and a benzene molecule is assumed to exist if the following distance and angular criteria are satisfied: For water-water hydrogen bonds, the O-O and O-H distances should be less than the cut-off distances R_c^{OO} and R_c^{OD} where the cut-off distances are: $R_c^{OO} = 3.5$ Å and $R_c^{OD} = 2.45$ Å. It may be noted that these cutoff distances R_c^{OO} and R_c^{OD} are essentially the positions of the first minimum of the oxygen-oxygen and oxygen-hydrogen RDFs, respectively. We

have also used an angular cut-off of 30° for the oxygen-oxygen-hydrogen angle[91,92,95]. Similarly, the cut-off values for benzene-oxygen (Bz-O) and benzene-hydrogen (Bz-D) distances are determined from the positions of first minimum of the benzene centre of mass to water oxygen and hydrogen RDFs and the values thus obtained are: $R_c^{Bz-O} = 3.6$ Å and $R_c^{Bz-D} = 3.0$ Å. We have not used any angular cut-off for benzene-water hydrogen bonds. The first solvation shell around benzene is defined up to a distance of 6.0 Å from the benzene centre of mass.

Previous studies suggested that small hydrophobic molecules induce ordering in the surrounding water by reducing the volume of the configuration space for hydrogen bonds[3]. A comprehensive way to study the hydrogen bonding picture in the anisotropic solvation shell of benzene is to calculate the time averaged network of hydrogen-bonds in various conical regions around the solute. The average number of hydrogen bonds per water molecule around benzene in the axial and equatorial regions, full solvation shell and also in bulk water are included in Table I. It is found that the average number of hydrogen bonds (HB) per water in the solvation shell and bulk solution differ only by a small factor. Slight differences are also found between the results of BLYP and BLYP-D functionals. The distributions of the average hydrogen bond numbers in different conical regions around benzene and also in the region beyond the first solvation shell (bulk) are shown in Figs.5(a)-(b). It is found that the fractions of water without a single hydrogen bond (NIL), single acceptor (A), double acceptor (AA), single donor (D) and double donor (DD) are negligibly small in the solvation shell. Hence, we focus primarily on the single acceptor single donor (AD), double acceptor single donor (AAD), single acceptor double donor (ADD) and double acceptor double donor (AADD) types of water molecules which are found to be present in significant fractions. It is found that relatively larger number of AAD type water molecules are present in the smaller axial conical regions and the relative population of AAD type water molecules decreases on increasing the angle of the axial conical regions. However, there are less AAD type water molecules present in smaller equatorial conical regions and their relative population increases for larger equatorial regions. While more of the ADD and AADD type water molecules are found for the smaller equatorial regions, the reverse scenario is found for the smaller axial regions. This shows that smaller equatorial regions, being in closer proximity to

the benzene plane, have more of ADD and AADD type water molecules compared to the smaller axial regions. In the equatorial regions, water molecules have to orient their oxygens towards benzene periphery to interact with deuterated hydrogens of C_6D_6 and this kind of configurations favor maximum number of donor HBs to maintain its hydrogen bonded network. In the smaller axial regions, such orientations are not preferred due to the influence of πH-bonding interaction. As a result, the axial water oxygens are capable of accepting more number of hydrogen bonds. In Fig.5(c), we have shown the average number of πH bonded water molecules. From Fig.5(c), it is seen that the AADD is the most stable configuration for these water molecules, i.e. tetrahedrally coordinated state with one hydrogen bond donated to benzene.

4 Dynamics of water molecules in the solvation shell of benzene

4.1 Rotational dynamics

The rotational motion of water molecules is closely related to the formation and breaking of hydrogen bonds. The orientational motion of solvent molecules is analyzed by calculating the OH vector orientational time correlation function, $C_l^{\rm OD}(t)$, in different conical regions around a benzene solute molecule. This function is defined by

$$C_l^{\rm OD}(t) = \frac{< P_l(\mathbf{u}_{\rm OD}(t) \cdot \mathbf{u}_{\rm OD}(0)) >}{< P_l(\mathbf{u}_{\rm OD}(0) \cdot \mathbf{u}_{\rm OD}(0)) >} \ , \tag{1}$$

where P_l is the Legendre polynomial of rank l and $\mathbf{u}_{\rm OD}$ is the unit vector which points along an OD bond of water molecules. In this work, we have calculated the time dependence of $C_l^{\rm OD}(t)$ for l = 1 and 2. Here we have plotted only the second-rank rotational functions $C_2^{\rm OD}(t)$ as these functions are directly related to experimentally measured time dependent rotational anisotropy of water molecules. The orientational correlation time, $\tau_l^{\rm OD}$, is defined as the time integral of orientational correlation function inside the solvation shell of benzene,

$$\tau_l^{\rm OD} = \int_0^\infty dt \ C_l^{\rm OD}(t) \ . \tag{2}$$

We calculated $\tau_l^{\rm OD}$ by explicit integration of the $C_l^{\rm OD}(t)$ from simulations and by calculating the integral for the tail part from fitted exponential functions. Fig.6(a) shows the decay of $C_2^{\rm OD}(t)$ for πH-bonded water OD vectors in $<$ 200 fs time range and Fig.6(b)

shows the dynamics in the long time region. We selectively calculated the orientational relaxation of an OD vector which was initially (at t = 0) πH-bonded to benzene and also that of the second OD vector of the same water molecule. The decay of $C_2^{\mathrm{OD}}(t)$ for πH-bonded OD vector is faster than the other OD of the same water molecule which is true for both BLYP-D and BLYP functionals. Moreover, in the sub-picosecond time scale regime, the πH-bonded OD vector shows faster decay than the other OD vector. This sub-picosecond regime of reorientational motion is related to the breaking and creation of hydrogen bonds due to libration, hence the short time decay reflects the strength of the hydrogen bond[96,97]. It is clear from Fig.6(a) that the πH-bonded OD vector performs larger amplitude librational motion than the other OD vector of the same water molecule. The orientational times for πH-bonded OD vector and the other OD vector of the same πH-bonded water molecule are included in Table II. The results show that the πH-bonded OD rotational relaxation is almost two times faster than that of the other OD vector of the same water molecule. Similar results are found for both the functionals although the actual time scales are found to be rather different for the two functionals. The general trends are consistent with recent experimental studies of πH-bonding in some aromatic compounds which reported that πH-bonded OH group readily reorients and translates[98–100].

In Figs.6(c)-(d), we have shown the decay of $C_2^{\mathrm{OD}}(t)$ for the OD vectors of water molecules in various axial and equatorial conical regions around the benzene solute. The water molecules initially present in a particular angular conical region are considered for calculations of rotational dynamics in that region. The second-rank orientational relaxation times for different axial and equatorial regions are included in Table III. We again note that the 90 ° axial and equatorial regions cover the total solvation shell around benzene, hence represent the same region. We found a fast orientational relaxation of water molecules in the smaller axial regions which then slow down for larger axial regions. However, in case of the equatorial regions, the rotational dynamics of water molecule is found to be slower for smaller equatorial regions and faster for the larger equatorial regions. On increasing the angles of the axial and equatorial conical regions of interest, the differences in the orientational dynamics are found to be more prominent for the BLYP functional than that for the BLYP-D functional.

The reason of faster dynamics of water molecules in the axial conical regions is that

the water molecules in small axial regions are mostly influenced by π-hydrogen bonding interaction. The πH-bonding, being a weaker interaction in comparison to water-water hydrogen bonding, gives rise to faster dynamics in the axial region. The water molecules which are πH-bonded to benzene show faster reorientational motion and tend to form H-bonds with other water molecules in the solvation shell which induce breaking of other water-water H-bonds in the axial region. Therefore, the benzene-water weak π-H bonding affects the water-water hydrogen bonding network and gives rise to faster dynamics in the axial region. However, in the small equatorial regions, water molecules are mostly influenced by C$-$D$\cdots$O hydrophobic interaction and water-water hydrogen bonding. Unlike the small axial regions, the water molecules in small equatorial regions tend to reorient slowly because of hydrophobic interactions and water-water H-bonds of both the OD groups of such water molecules. These different interactions in the axial and equatorial regions lead to different rotational dynamics of water molecules at the faces and edges of the benzene solute molecule. It is also found from the second-rank rotational functions that the overall dynamics of the solvation shell water molecules is slower than that of the bulk. This slowing down can be attributed to the enhancement of water structure around the hydrophobic solute as discussed in Section 3.3.

4.2 Orientational Jumps and Switching of Hydrogen Bonds

It was shown earlier that the reorientation of water takes place mainly through large amplitude angular jumps[101,102]. The reorientation and hydrogen bond cleavage of water molecules occur concertedly and not successively[101,102]. The presence of orientational jumps have also been reported in other liquids such as molten acetamide[103,104]. In the present study, we have investigated the rotational behavior and hydrogen bond switching mechanism for πH-bonded water. In particular, we have looked at the dynamics of πH-bonds from the perspective of jump mechanism. To the best of our knowledge, this is the first study which examines if a πH-bonded water reorients in small diffusive steps or via large amplitude angular jumps. We examine all the πH-bond switches from benzene to another water. In Fig.7(a), the O*D* represents the πH-bonded mode of water and D_2O^b is the water molecule to which the πH-bonded O*D* mode would switch its hydrogen bond. We denote the relative distances of benzene centre of mass and πH-bonded water as O*$\cdots$Bz and πH-bonded water to D_2O^b as O*$\cdots O^b$. These notations are similar to

those used for water-water and water-ion H-bond switches[101,102]. We look at the rotation of O*D* from benzene to D_2O^b. It is found that the πH bonded O*D* mode, during its librational motion above the benzene ring, comes across the instances when it is almost equidistant to benzene and O^b. This equidistant D*, within hydrogen bonding distance ranges, is in a bifurcated hydrogen bonding state and this state can be considered as the transition state for H-bond switching. The transition state is an unstable state and the O*D* then changes its hydrogen bond partner from benzene to water through large amplitude angular jump of around 60-70 °. An almost similar jump amplitude was found for water-water angular jumps[101].

In Fig.7(b), We have shown the variation of O*$\cdots$Bz and O*$\cdots O^b$ distances as the system passes through the πH-bonded state of O*D* to the formation of hydrogen bond with D_2O^b. Results are shown for both the BLYP and BLYP-D functionals. The time is set to zero at the switching event of D* from Bz to O^b. The average distance of O*$\cdots$Bz in the πH bonded state is found to be 3.3 Å and the average O*$\cdots O^b$ distance in hydrogen bonding state is found to be 2.8 Å . The jump angle (θ) is defined as the angle between the angle bisector of BzO*O^b plane and the projection of D* on the BzO*O^b plane, as shown in Fig.7(c) . It is found that the πH-bonded O*D* mode performs a switch of its hydrogen bond from benzene to water via a large amplitude angular jump of around 60-70 °. There is very little ($\sim$ 2%) πH-bond switching/reorientation occurrence through small diffusive steps to change its hydrogen bond.

The number of hydrogen bonds accepted by O*, Benzene and O^b are shown in Fig.7(d) . It is found that the average number of π-hydrogen-bonds accepted by the benzene molecule before t = 0 is $\sim$ 1.5 and then it decays to $\sim$ 0.5 as a πH-bond switches its partner. The average number of hydrogen bonds accepted by O^b before t = 0 is 1.0 and it is 2.0 after t = 0 as the O*D* forms a hydrogen bond with O^b. The HB number, however, remains constant for O*. This shows that the πH-bonded O* has double acceptor nature and it remains in that double acceptor state after the πH-bond switching event. On the other hand, before t = 0, the O^b is in a single acceptor state which is ready to accept another hydrogen bond. We have also calculated the number of donor hydrogen bonds of D′ which is the second deuterated hydrogen of the πH-bonded water. It is found that its hydrogen bond remains intact during the πH-bond switching. So, it is clear from our calculations that although the πH-bonded O*D* mode performs higher degree of librational motion, it

changes its partner from benzene to water via large amplitude rotational jump mechanism.

We have also looked at the H-bond switching of water molecules in the benzene solvation shell and in bulk water. It is found that the changes in distances and jump angles for H-bond switches in the solvation shell and bulk are very close to those reported for pure water[101,102]. However, the number of switches per water is found to be less in the solvation shell which can be linked to an overall slower reorientational motion of water molecules in the solvation shell[105] due to hydrophobic interactions with the solute. The excluded volume of the solute may also hinder the reorientational motion[106]. The enhanced hydrogen bonded structure found in the solvation shell may also be one of the reasons for the slower reorientational motion of water around the benzene solute.

4.3 Hydrogen bond dynamics

We have studied the dynamics of benzene-water and water-water hydrogen bonds by using the population correlation function approach[88–95,107–111]. The HBs are defined by using a set of geometric criteria as described in Section 3. We define two hydrogen-bond population variables: h(t) and H(t), where h(t) is unity when a particular water-water (W-W) or benzene-water (B-W) pair is hydrogen-bonded at time t and zero otherwise. H(t) = 1 if a particular W-W or B-W pair remains continuously hydrogen-bonded from t = 0 to time t and it is zero otherwise. We calculate the continuous hydrogen-bond time correlation function $S_{\rm HB}(t)$ which is defined as[90–95,107]

$$S_{\rm HB}(t) = \frac{< h(0)H(t) >}{< h(0)^2 >} \ , \tag{3}$$

where $< ... >$ denotes an average over all chosen W-W or B-W pairs. $S_{\rm HB}(t)$ describes the probability that an initially hydrogen bonded W-W or B-W pair remains bonded at all times up to t. The associated integrated relaxation time τ_{HB} gives the average lifetime of a hydrogen bond between water molecules or between benzene and water molecule present in the region of interest. The most probable configuration found for a πH-bonded water molecule is with its O*D* bonded to benzene and other O*D′ bonded to a water molecule. Therefore, in Fig.8(a) we have plotted the continuous hydrogen bond correlation functions separately for benzene-D*O* and OD′-water pairs. The average lifetimes for πH-bond and the OD′-water hydrogen bond are given in Table IV. It is found that the πH-bond lifetime is relatively very small than that of water-water hydrogen bonds which means that the

former is a weaker hydrogen bond. The benzene-water hydrogen bond life time is found to be slightly longer for the BLYP-D functional compared to its value for the BLYP functional which can be attributed to the effects of dispersion interactions.

Fig.8(b) shows the decay of hydrogen bond correlations of water-water pairs in different axial conical regions around the benzene solute. The integrated relaxation times for benzene-water and water-water HBs are included in Table V for different axial and equatorial regions. It is found that the average H-bond lifetimes of water molecules present in the axial region are less than that of water molecules in the equatorial regions. The equatorial water molecules have longer survival time of hydrogen bonds than the bulk and, as a result, the overall solvation shell hydrogen bond dynamics is found to be slower than bulk hydrogen bonds. Although quantitatively different values are found for the BLYP and BLYP-D functionals, the qualitative trend of the hydrogen bond dynamics remains similar for both the functionals.

5 Dynamics of Vibrational Frequency Fluctuations

We have calculated time dependent stretch frequencies of the OD modes of deuterated water molecules by a time series analysis of the simulated trajectories[47,70,85]. We then separated the frequencies of OD modes for water in πH-bonded, axial, equatorial, full solvation shell and bulk regions. The time averaged distributions of these frequencies are shown in Fig.9(a). We have normalized all sets of frequencies to the same scale for clarity of their comparisons. The average frequency of the πH-bonded OD modes is found to be $2521\,\mathrm{cm}^{-1}$ which is about $50\,\mathrm{cm}^{-1}$ red shifted from the average frequency of the dangling OD modes ($2570\,\mathrm{cm}^{-1}$) found by the same level of calculations[112]. This frequency shift of $\sim 50\,\mathrm{cm}^{-1}$ for πH-bonded OD modes is in excellent agreement with the results of recent experiments[8]. The axial, equatorial, solvation shell and bulk OD modes have average frequencies around $2375\,\mathrm{cm}^{-1}$ which is close to the average frequency of OD modes in pure water ($2380\,\mathrm{cm}^{-1}$)[70]. This shows that most of the water-water hydrogen bonded OD modes are red shifted compared to the πH-bonded OD modes. The OD mode distribution of the axial region has a shoulder around $2500\,\mathrm{cm}^{-1}$ which is a manifestation of AAD type water molecules in the axial regions as discussed earlier. This shoulder is less pronounced in all other regions such as the equatorial, full solvation shell and bulk

OD mode distributions. The OD bond frequencies are greatly influenced by the hydrogen bonded state of the OD groups. The stronger the hydrogen bond, higher will be the redshift in OD stretching frequencies. We also note that the frequency distributions are found to be similar for the BLYP-D and BLYP functionals.

Our main focus here is to study the decay of frequency fluctuations and its correlations with the hydrogen bond dynamics. The frequency time correlation function is defined as

$$C_\omega(t) = \frac{\langle \delta\omega(t)\delta\omega(0)\rangle}{\delta\omega(0)^2} \ , \tag{4}$$

where $\delta\omega$ (t) is the fluctuation from the average stretch frequency at time t. The average of this equation is over those modes which were present in the respective regions at the initial time. The frequency correlation function captures the time dependence of vibrational frequency changes due to fluctuations in the surrounding environment [70,112–125]. The results of the frequency correlation functions for the solvation shell and bulk water are shown in Fig.9(b) for both BLYP and BLYP-D functionals. The frequency correlation functions are fitted by a bi-exponential function and the corresponding relaxation times are included in Table VI. The short time scale of frequency correlations originate from the underdamped motion of intact hydrogen bonded pairs and the long time decay corresponds to the hydrogen bond breaking dynamics. It is found that the frequency relaxation in the solvation shell is slower than that in the bulk for both the BLYP-D and BLYP functionals which is similar to the dynamics of hydrogen bond fluctuations discussed in the previous section. Therefore, the slower relaxation of hydrogen bonds in the solvation shell of benzene compared to that in bulk is also captured in the fluctuations of stretch frequencies of water in the said regions.

6 Summary and conclusions

In the present study, we have investigated the structural and dynamical behavior of water molecules in different parts of the anisotropic hydration shell of a benzene solute molecule at room temperature. We have looked at various quantities such as benzene-water radial distribution functions in different conical regions, radial/angular correlations, water-water inter-particle distance/angle distributions, diffusion and orientational relaxation, rotational jumps of π-hydrogen-bonded water molecules and switching from π-hydrogen-bonds to water-water hydrogen bonds, hydrogen bond relaxation and also

frequency time correlations in different parts of the solvation shell. The current study is based on *ab initio* molecular dynamics simulations of water containing a benzene solute at ambient conditions. Both BLYP and the dispersion corrected BLYP-D functionals are used for calculations of the quantum electronic structure, energies and forces of the benzene-water system.

The structure and dynamics of hydration shell water molecules around benzene are found to be highly anisotropic as revealed by the radial distribution functions of different conical regions, joint radial/angular distribution functions and also dynamical correlations in different conical regions. Water molecules present in the axial regions of benzene are found to have the preferred orientation of one OD bond pointing toward the benzene ring whereas water molecules located in the equatorial region tend to orient their dipoles away from the benzene ring. We have also calculated the benzene-water dimer potential energy curves for many different orientations of water along the axial and equatorial directions for both BLYP and BLYP-D functionals. The simulation results of the hydration shell structure of benzene, particularly the benzene-water RDFs in the axial and equatorial regions, are discussed based on the differences in the benzene-water potential energies for different orientations and also for different functionals. The inter-particle correlations show an enhanced water structure in the solvation shell of benzene compared to that between the solvation shell and bulk and also within the bulk molecules.

On average, a single πH-bond is found to be formed between the benzene solute and its surrounding water. The πH-bond of water-benzene pair is a weaker interaction than water-water hydrogen bonds. The πH-bonded water molecules show faster rotational and translational dynamics which in turn affect the overall dynamics of the axial region of the solvation shell. The water molecules in the axial region are found to show faster dynamics than the equatorial water molecules. The lifetime of πH-bond is found to be shorter than water-water H-bonds. Still, the πH-bonded water molecules are found to follow jump mechanism of reorientation to change its hydrogen bonded partner like those hydrogen bonded to other water molecules. The stretch frequency of the πH-bonded OD bond is found to be red shifted by about $50\,\mathrm{cm}^{-1}$ which is in good agreement with recent experiments[8].

Acknowledgment

Financial support from the Department of Science and Technology (DST) and Council of Scientific and Industrial Research (CSIR), Government of India, is gratefully acknowledged.

TABLE I. Average number of hydrogen bonds per water molecule in the solvation shell and bulk. The axial and equatorial regions correspond to those with conical angle of 45°. The standard deviations in the hydrogen bond numbers are found to vary from 0.9% (for bulk) to 2% (for axial and equatorial solvation shells) of the respective average values reported in the Table.

Functional	Axial	Equatorial	Solvation Shell	Bulk
BLYP-D	3.60	3.64	3.62	3.69
BLYP	3.68	3.71	3.70	3.79

TABLE II. Values of the second rank orientational relaxation times (τ_2) of the OD vector which is π-hydrogen bonded to benzene and of the second OD vector of the same π-hydrogen bonded water. The relaxation times are expressed in units of ps. The standard deviations in the relaxation times are found to be in the range of 3.5-4.0% of the values reported in the Table.

OD mode		τ_2^{OD}
BLYP-D	π-H-bonded OD	1.74
	Second OD of the same water	4.43
BLYP	π-H-bonded OD	3.29
	Second OD of the same water	5.89

TABLE III. Second rank orientational relaxation times (τ_2) of the OD vectors of water molecules in the conical regions of the hydration shell of a benzene solute molecule. The relaxation times are expressed in units of ps. $\tau_2^{x^\circ}$ means τ_2 of water in a conical region of the solvation shell characterized by the conical angle of x°. The standard deviations in the relaxation times are found to be in the range of 2.5% (for τ_2^{bulk}) to 4.2% (for $\tau_2^{15^\circ}$) of the respective values reported in the Table.

Conical region		$\tau_2^{15^\circ}$	$\tau_2^{30^\circ}$	$\tau_2^{45^\circ}$	$\tau_2^{60^\circ}$	$\tau_2^{75^\circ}$	$\tau_2^{90^\circ}$	τ_2^{bulk}
BLYP-D	Axial	3.48	4.06	4.75	5.14	5.37	5.43	4.93
	Equatorial	5.78	5.78	5.71	5.63	5.54		
BLYP	Axial	10.62	10.92	11.05	11.94	12.46	13.34	12.02
	Equatorial	18.34	17.52	16.17	15.25	14.81		

TABLE IV. Hydrogen bond lifetimes of the benzene-water π-hydrogen bonded (O*D*$\cdots$benzene) and the water-water hydrogen bonded (O*D$'\cdots$water) pairs in the units of ps. The standard deviations in the hydrogen bond lifetimes are found tio be 3.5% for πH-bonds and 2% for water-water H-bonds.

Hydrogen bond		τ_{HB}
BLYP-D	Benzene-Water π-H-bond of O*D*	0.35
	Water-Water HB of O*D$'$	1.66
BLYP	Benzene-Water π-H-bond of O*D*	0.30
	Water-Water HB of O*D$'$	3.29

TABLE V. Hydrogen bond lifetimes (τ_{HB}) of water molecules in different conical regions of the solvation shell of benzene in units of ps. $\tau_{HB}^{x^\circ}$ means the τ_{HB} of water in a conical region of the solvation shell characterized by the conical angle of x°. The standard deviations in the hydrogen bond lifetimes are found to vary from 1.8% (for τ_{HB}^{bulk}) to 2.6% (for $\tau_{HB}^{15^\circ}$) of the respective values reported in the Table.

Conical region		$\tau_{HB}^{15^\circ}$	$\tau_{HB}^{30^\circ}$	$\tau_{HB}^{45^\circ}$	$\tau_{HB}^{60^\circ}$	$\tau_{HB}^{75^\circ}$	$\tau_{HB}^{90^\circ}$	τ_{HB}^{bulk}
BLYP-D	Axial	1.68	1.75	1.79	1.83	1.84	1.84	1.77
	Equatorial	1.95	1.94	1.92	1.90	1.86		
BLYP	Axial	3.53	3.54	3.72	3.75	3.84	3.91	3.76
	Equatorial	4.24	4.15	4.11	4.01	3.95		

TABLE VI. Relaxation times (τ) and weights (a) of the frequency correlations of OD modes of water in the solvation shell and bulk. The results are averaged over OD modes of those water molecules which are present in the respective regions at the initial time. The standard deviations in the relaxation times are in the range of 2.2-2.8% of the values reported in the Table.

Region	Functional	τ_1 (ps)	τ_2 (ps)	a_1	a_2
solvation shell	BLYP-D	0.06	2.8	0.65	0.35
	BLYP	0.07	3.7	0.67	0.33
Bulk	BLYP-D	0.04	2.2	0.63	0.37
	BLYP	0.05	3.0	0.64	0.36

References

[1] W. Blokzijl and J. Engberts, *Angew. Chem., Int. Ed. Engl.*, 1993, **32**, 1545.

[2] P. Ball, *Chem. Rev.*, 2008, **108**, 74.

[3] D. Chandler, *Nature(London)*, 2005, **437**, 640.

[4] A. Ben-Naim, *Hydrophobic Interaction*, Plenum Press, New York, 1980.

[5] L. R. Pratt and D. Chandler, *J. Chem. Phys.*, 1980, **73**, 3430.

[6] S. Suzuki, P. G. Green, R. E. Bumgarner, S. Dasgupta, W. A. Goddard III and G. A. Blake, *Science*, 1992, **257**, 942.

[7] T. Steiner and G. Koellner, *J. Mol. Biol.*, 2001, **305**, 535.

[8] K. P. Gierszal, J. G. Davis, M. D. Hands, D. S. Wilcox, L. V. Slipchenko and D. Ben-Amotz, *J. Phys. Chem. Lett.*, 2011, **2**, 2930.

[9] A. J. Gotch and T. S. Zwier, *J. Chem. Phys.*, 1992, **96**, 3388.

[10] G. C. Pimentel and A. L. McClellan, *The Hydrogen Bond*, W. H. Freeman, San Francisco, 1960.

[11] A. Engdahl and B. Nelander, *J. Phys. Chem.*, 1985, **89**, 2860.

[12] T. S. Zwier, *Annu. Rev. Phys. Chem.*, 1996, **47**, 205.

[13] R. N. Pribble, A. W. Garrett, K. Haber and T. S. Zwier, *J. Chem. Phys.*, 1995, **103**, 531.

[14] C. J. Gruenloh, J. R. Carney, C. A. Arrington, T. S. Zwier, S. Y. Fredericks and K. D. Jordan, *Science*, 1997, **276**, 1678.

[15] P. Chakrabarti and R. Bhattacharyya, *Prog. Biophys. Mol. Biol.*, 2007, **95**, 83.

[16] P. N. Perera, K. R. Fega, C. Lawrence, E. J. Sundstrom, J. Tomlinson-Phillips and D. Ben-Amotz, *P. Natl. Acad. Sci. U.S.A.*, 2009, **106**, 12230.

[17] A. Laaksonen, P. Stilbs and R. E. Wasylishen, *J. Chem. Phys.*, 1998, **108**, 455.

[18] P. Schravendijk and N.F.A. van der Vegt, *J. Chem. Theory Comput.*, 2005, **1**, 643.

[19] T. M. Raschke and M. Levitt, *P. Natl. Acad. Sci. U.S.A.*, 2005, **102**, 6777.

[20] T. M. Raschke and M. Levitt, *J. Phys. Chem. B*, 2004, **108**, 13492.

[21] M. P. S. Mateus, N. Galamba and B. J. C. Cabral, *J. Chem. Phys.*, 2012, **136**, 014507.

[22] A. Choudhary and A. Chandra, *J. Phys. Chem. B*, 2015, **119**, 8600.

[23] M. Allesch, E. Schwegler and G. Galli, *J. Phys. Chem. B*, 2007, **111**, 1081.

[24] M. Allesch, F. C. Lightstone, E. Schwegler and G. Galli, *J. Chem. Phys.*, 2008, **128**, 014501.

[25] P. Agre, *Angew. Chem. Int. Ed.*, 2004, **43**, 4278.

[26] D. D. Kozono, M. Yasui, L. S. King and P. J. Agre, *Clin. Invest.*, 2002, **109**, 1395.

[27] M. Kumar, M. Grzelakowski, J. Zilles, M. Clark and W. Meier, *Proc. Natl. Acad. Sci. U. S. A.*, **104**, 20719 (2007).

[28] G. Hummer, J. C. Rasaiah, and J. P. Noworyta, *Nature*, 2001, **414**, 188.

[29] D. Takaiwa, I. Hatano, K. Koga and H. Tanaka, *Proc. Natl. Acad. Sci. U. S. A.*, 2008, **105**, 39.

[30] T. A. Pascala, W. A. Goddarda and Y. Junga, *Proc. Natl. Acad. Sci. U. S. A.*, 2011, **108**, 11794.

[31] R. Natarajan, J. P. H. Charmant, A. G. Orpen and A. P. Davis, *Angew. Chem. Int. Ed.*, 2010, **49**, 5125.

[32] R. Prohens, M. Font-Bardia and R. Barbas, *CrystEngComm*, 2013, **15**, 845.

[33] R. Car and M. Parrinello, *Phys. Rev. Lett.*, 1985, **55**, 2471.

[34] D. Marx and J. Hutter, *Ab Initio Molecular Dynamics: Basic Theory and Advanced Methods*, Cambridge University Press, Cambridge, 2009.

[35] H. S. Frank and M. W. Evans, *J. Chem. Phys.*, 1945, **13**, 507.

[36] Y. Rezus and H. J. Bakker, *Phys. Rev. Lett.*, 2007, **99**, 148301.

[37] W. Kohn and L. J. Sham, *Phys. Rev.*, 1965, **140**, A1133.

[38] J. Hutter, A. Alavi, T. Deutsch, M. Bernasconi, S. Goedecker, D. Marx, M. Tuckerman and M. Parrinello, *CPMD program*, MPI für Festkörperforschung and IBM Zurich Research Laboratory.

[39] N. Troullier and J. L. Martins, *Phys. Rev. B*, 1991, **43**, 1993.

[40] A. D. Becke, *Phys. Rev. A*, 1988, **38**, 3098.

[41] C. Lee, W. Yang and R. G. Parr, *Phys. Rev. B*, 1988, **37**, 785.

[42] S. Grimme, *J. Comput. Chem.*, 2004, **25**, 1463.

[43] S. Grimme, *J. Comput. Chem.*, 2006, **27**, 1787.

[44] S. Grimme, J. Antony, T. Schwabe and C. Mück-Lichtenfeld, *Org. Biomol. Chem.*, 2007, **5**, 741.

[45] K. Laasonen, M. Sprik, M. Parrinello and R. Car, *J. Chem. Phys.*, 1993, **99**, 9080.

[46] M. Sprik, J. Hutter and M. Parrinello, *J. Chem. Phys.*, 1996, **105**, 1142.

[47] B. S. Mallik, A. Semparithi and A. Chandra, *J. Phys. Chem. A*, 2008, **112**, 5104.

[48] P. L. Silvestrelli and M. Parrinello, *J. Chem. Phys.*, 1996, **105**, 1142.

[49] P. L. Silvestrelli and M. Parrinello, *Phys. Rev. Lett.*, 1999, **82**, 3308.

[50] P. L. Silvestrelli and M. Parrinello, *J. Chem. Phys.*, 1999, **111**, 3572.

[51] P. L. Silvestrelli, M. Bernasconi and M. Parrinello, *Chem. Phys. Lett.*, 1997, **277**, 478.

[52] M. Krack, A. Gambirasio and M. Parrinello, *J. Chem. Phys.*, 2002, **117**, 9409.

[53] B. Chen, I. Ivanov, M. L. Klein and M. Parrinello, *Phys. Rev. Lett.*, 2003, **91**, 215503.

[54] S. Izvekov and G. A. Voth, *J. Chem. Phys.*, 2002, **116**, 10372.

[55] M. Boero, K. Terakura, T. Ikeshoji, C. C. Liew and M. Parrinello, *Phys. Rev. Lett.*, 2000, **85**, 3245.

[56] M. Boero, K. Terakura, T. Ikeshoji, C. C. Liew and M. Parrinello, *J. Chem. Phys.*, 2001, **115**, 2219.

[57] M. Boero, *J. Phys. Chem. A*, 2007, **111**, 12248.

[58] D. Marx, M. E. Tuckerman, J. Hutter and M. Parrinello, *Nature (London)*, 1999, **397**, 601.

[59] M. E. Tuckerman, D. Marx and M. Parrinello, *Nature (London)*, 2002, **417**, 925.

[60] B. Kirchner, J. Stubbs and D. Marx, *Phys. Rev. Lett.*, 2002, **89**, 215901.

[61] J. M. Heuft and E. J.Meijer, *Phys. Chem. Chem. Phys.*, 2006, **8**, 3116 (2006).

[62] M. Cavallari, C. Cavazzoni and M. Ferrario, *Mol. Phys.*, 2004, **102**, 959.

[63] T. Ikeda, M. Hirata and T. Kimura, *J. Chem. Phys.*, 2003, **119**, 12386.

[64] K. Leung and S. B. Rempe, *J. Am. Chem. Soc.*, 2004, **126**, 344.

[65] L. M. Ramaniah, M. Barnasconi and M. Parrinello, *J. Chem. Phys.*, 1999, **111**,1587.

[66] A. P. Lyubartsev, K. Laasonen and A. Laaksonen, *J. Chem. Phys.*, 2001, **114**, 3120.

[67] M.-P. Gaigeot and M. Sprik, *J. Phys. Chem. B*, 2004, **108**, 7458.

[68] M. Masia, *J. Chem. Phys.*, 2008, **128**, 184107.

[69] M. Masia, H. Forbert and D. Marx, *J. Phys. Chem. A*, 2007, **111**, 12181.

[70] B. S. Mallik, A. Semparithi and A. Chandra, *J. Chem. Phys.*, 2008, **129**, 194512.

[71] J. Schmidt, J. VandeVondele, I.-F. Kuo, D. Sebastiani, J. I. Siepmann, J. Hutter and C. J. Mundy, *J. Chem. Phys. B*, 2009, **113**, 11959.

[72] M. J. McGrath, I.-F. Kuo and J. I. Siepmann, *Phys. Chem. Chem. Phys.*, 2011, **13**, 19943.

[73] M. J. McGrath, I.-F. Kuo, J. N. Ghogomu, C. J. Mundy and J. I. Siepmann, *J. Phys. Chem. B*, 2011, **115**, 11688.

[74] R. Jonchiere, A. P. Sietsonen, G. Ferlat, A. M. Saitta and R. Vuilleumier, *J. Chem. Phys.*, 2011, **135**, 154503.

[75] J. Wang, G. Roman-Perez, J. M. Soler, E. Artacho and M.-V. Fernandez-Serra, *J. Chem. Phys.*, 2011, **134**, 024516.

[76] S. Yoo and S. S. Xantheas, *J. Chem. Phys.*, 2011, **134**, 121105.

[77] I-Chun Lin, A. P. Sietsonen, I. Tavernelli and U. Rothlisberger, *J. Chem. Theory Comput.*, 2012, **8**, 3902.

[78] A. Bankura, A. Karmakar, V. Carnevale, A. Chandra and M. Klein, *J. Phys. Chem. C*, 2014, **118**, 29401.

[79] A. Karmakar and A. Chandra, *Chem. Phys.*, 2015, **448**, 1.

[80] S. Grimme, J. Antony, S. Ehrlich and H. Kreig, *J. Chem. Phys.*, 2010, **132**, 154104.

[81] See the Supplementary Information available online with this article for justifications of using density functionals and other parameters of the current simulations, Tables containing results of binding energies and various structural parameters of the benzene-water dimer for different levels of calculations, and also figures containing results of Fictitious electronic temperature, ionic temperature and extended Hamiltonian, illustration of conical regions and tilt angles, coordination and πH-bond number distributions, radial/angular functions and inter-particle distance/angle distributions.

[82] H. J. C. Berendsen, J. R. Grigera and T. P. Straatsma, *J. Phys. Chem.*, 1987, **91**, 6269.

[83] W. L. Jorgensen, D. S. Maxwell and J. Tirado-Rives, *J. Am. Chem. Soc.*, 1996, **118**, 11225.

[84] M. Fuentes, P. Guttorp and P. D. Sampson, in *Stastical Methods for Spatio-Temporal Systems* , ed. B. Finkenstädt, L. Held, and V. Isham, Chapman & Hall/CRC, Boca Raton, 2007, Chap. 3, 78.

[85] L. V. Vela-Arevalo and S. Wiggins, *Int. J. Bifurcation. Chaos Appl. Sci. Eng.*, 2001, **11**, 1359.

[86] A. Semparithi and S. Keshavamurthy, *Phys. Chem. Chem. Phys.*, 2003, **5**, 5051.

[87] K. R. Gallagher and K. Sharp, *J. Am. Chem. Soc.*, 2003, **125**, 9853.

[88] A. Luzar and D. Chandler, *Phys. Rev. Lett.*, 1996, **76**, 928.

[89] A. Luzar and D. Chandler, *Nature (London)*, 1996, **379**, 55.

[90] A. Luzar, *J. Chem. Phys.*, 2000, **113**, 10663.

[91] A. Chandra, *Phys. Rev. Lett.*, 2000, **85**, 768.

[92] A. Chandra, *J. Phys. Chem. B*, 2003, **107**, 3899.

[93] S. Balasubramanian, S. Pal and B. Bagchi, *Phys. Rev. Lett.*, 2002, **89**, 115505.

[94] S. Chowdhuri and A. Chandra, *Phys. Rev. E*, 2002, **66**, 041203.

[95] B. S. Mallik and A. Chandra, *J. Chem. Phys.*, 2006, **125**, 234502.

[96] D. E. Moilanen, E. E. Fenn, Y.-S. Lin, J. L. Skinner, B. Bagchi and M. D. Fayer, *Proc. Natl. Acad. Sci. U.S.A.*, 2008, **105**, 5295.

[97] D. Laage and J. T. Hynes, *Chem. Phys. Lett.*, 2006, **433**, 80.

[98] J. Zheng, K. Kwak, J. Asbury, X. Chen, I. R. Piletic and M. D. Fayer, *Science*, 2005, **309**, 1338.

[99] D. E. Rosenfeld, K. Kwak, Z. Gengeliczki and M. D. Fayer, *J. Phys. Chem. B*, 2010, **114**, 2383.

[100] D. E. Rosenfeld, Z. Gengeliczki and M. D. Fayer, *J. Phys. Chem. B*, 2009, **113**, 13300.

[101] D. Laage and J. T. Hynes, *Science*, 2006, **311**, 832.

[102] D. Laage and J. T. Hynes, *J. Phys. Chem. B*, 2008, **112**, 14230.

[103] S. Das, R. Biswas and B. Mukherjee, *J. Phys. Chem. B*, 2015, **119**, 274.

[104] S. Das, R. Biswas and B. Mukherjee, *J. Phys. Chem. B*, 2015, **119**, 11157.

[105] A. A. Bakulin, M. S. Pshenichnikov, H. J. Bakker and C. Petersen *J. Phys. Chem. A*, 2011, **115**, 1821.

[106] D. Laage, G. Stirnemann and J. T. Hynes, *J. Phys. Chem. B*, 2009, **113**, 2428.

[107] D. Rapaport, *Mol. Phys.*, 1983, **50**, 1151.

[108] H. Xu and B. J. Berne, *J. Phys. Chem. B*, 2001, **105**, 11929.

[109] H. Xu, H. A. Stern and B. J. Berne, *J. Phys. Chem. B*, 2002, **106**, 2054.

[110] S. Raugei and M. L. Klein, *J. Am. Chem. Soc.*, 2001, **123**, 9484.

[111] S. Raugei and M. L. Klein, *J. Chem. Phys.*, 2002, **116**, 196.

[112] J. Roy Choudhuri and A. Chandra *J. Chem. Phys.*, 2014, **141**, 194705.

[113] H. J. Bakker and J. L. Skinner, *Chem. Rev.*, 2010, **110**, 1498.

[114] H. J. Bakker, M. F. Kropman, A. W. Omta and S. Woutersen, *Phys. Scr.*, 2004, **69**, C14.

[115] J. B. Asbury, T. Steinel, C. Stromberg, S. A. Corcelli, C. P. Lawrence, J. L. Skinner and M. D. Fayer, *J. Phys. Chem. A*, 2004, **108**, 1107.

[116] E. T. J. Nibbering and T. Elsaesser, *Chem. Rev.*, 2004, **104**, 1887.

[117] C. J. Fecko, J. D. Eaves, J. J. Loparo, A. Tokmakoff and P. L. Geissler, *Science*, 2003, **301**, 1698.

[118] C. J. Fecko, J. J. Loparo, S. T. Roberts and A. Tokmakoff, *J. Chem. Phys.*, 2005, **122**, 054506.

[119] D. Chakraborty and A. Chandra, *J. Chem. Phys.*, 2011, **135**, 114510.

[120] J. L. Skinner, B. M. Auer and Y. S. Lin, *Adv. Chem. Phys.*, 2009, **142**, 59.

[121] R. Rey, K. B. Moller and J. T. Hynes, *J. Phys. Chem. A*, 2002, **106**, 11993.

[122] K. B. Moller, R. Rey and J. T. Hynes, *J. Phys. Chem. A*, 2004, **108**, 1275.

[123] C. P. Lawrence and J. L. Skinner, *Chem. Phys. Lett.*, 2003, **369**, 472.

[124] C. P. Lawrence and J. L. Skinner, *J. Chem. Phys.*, 2003, **117**, 8847.

[125] C. P. Lawrence and J. L. Skinner, *J. Chem. Phys.*, 2003, **118**, 264.

FIGURES

Figure 1. The axial and equatorial regions around a benzene solute molecule. The angle θ of an axial cone is the angle with the principal axis of C_6 symmetry.

Figure 2. The Bz-O and Bz-D radial distribution functions for the axial and equatorial conical regions around the benzene solute molecule. Bz means the centre of mass of the benzene molecule. The solid lines are for the BLYP-D functional and the dotted lines are for the BLYP functional.

Figure 3. The Bz-O radial distribution functions for the 15° axial and equatorial conical regions around the benzene solute molecule. The solid and dashed lines are for the BLYP-D and BLYP functionals, espectively. (a) Representative benzene-water configurations are shown in the 15^o axial conical shell at distances of 3.1-3.4, 3.7-3.9 and 4.8-6.0 Å from Bz. (b) Representative benzene-water configurations are shown in the 15^o equatorial conical shell at distances of 4.8-5.2 and 6.2-7.0 Å from Bz.

Figure 4. The benzene-water binding energy (kcal/mol) curves for different orientations of water along the (a) axial and (b) equatorial directions. The angle on the X-axis is that of the OH bond (with circled hydrogen) with respect to the C_6 axis of benzene for (a) axial benzene-water dimers and (b) with respect to a CH bond of benzene in the equatorial plane for equatorial benzene-water dimers. The negative angle is for anticlockwise rotation and the positive angle is for clockwise rotation of the OH bond with circled hydrogen. (a) The oxygen of water is placed at 3.4 Å from the centre of mass of the benzene (Bz) along the C_6 axis and (b) the water oxygen is placed at 5.0 Å from Bz along a CH axis.

Figure 5. The distributions of different hydrogen bond donor (D) and acceptor (A) states of water molecules in the axial and equatorial conical regions of the benzene solvation shell. The population is calculated on percentage basis considering all water molecules in a given region. The color filled bars are for the BLYP-D functional and empty bars are for the BLYP functional. (a) Population of water in different H-bonded states in the

axial conical regions (b) Population of water in different H-bonded states in the equatorial conical regions (c) Population of π-hydrogen bonded water molecules in different H-bonded states.

Figure 6. The orientational time correlation functions of the π-hydrogen bonded OD and other OD vector of the same water in the axial region of benzene solvation shell in the (a) short-time and (b) long-time regions of decay. (c) Orientational correlation functions of OD vectors of water molecules in different axial regions. The solid curves are for the BYLP-D functional and the corresponding dashed curves in the same color are for the BYLP functional. (d) Orientational correlation functions of OD vectors of water molecules in different equatorial regions. The solid curves are for the BYLP-D functional and the corresponding dashed curves in the same color are for the BYLP functional.

Figure 7. Successive steps of the concerted process of breaking of a benzene-water π-hydrogen-bond and formation of a water-water (W-W) hydrogen bond. (a) Initially, D* is π-hydrogen-bonded to benzene and D_2O_b is located further away from benzene. In the transition state, D* becomes almost equidistant from benzene and O_b and then D* flips from benzene to O_b. (b) Time evolutions of the O*$\cdots$Bz (green curve) and O*$\cdots O_b$ (blue) distances are plotted. (c) The jump angle θ is defined as the angle between the angle bisector of BzO*O^b plane and the projection of D* on the BzO*O^b plane. The jump angles for π-hydrogen-bond exchange events are plotted. (d) ${n_r}^{O^*}$, ${n_r}^{Bz}$, ${n_r}^{O^b}$ are the number of accepted hydrogen bonds by O*, benzene and O_b, respectively. These quantities are plotted in green, blue and maroon colors, respectively. ${n_d}^{D'}$ represents the number of hydrogen bonds donated by D$'$ (other hydrogen of the π-hydrogen-bonded water). The solid and dashed curves correspond to the results of BYLP-D and BYLP functionals, respectively.

Figure 8. Time dependence of the (a) continuous hydrogen bond correlation function $S_{HB}(t)$ of π-hydrogen-bond and OD$'$ water-water hydrogen bonds, (b) Continuous hydrogen bond correlation function $S_{HB}(t)$ between two water molecules in the axial regions. The solid curves are for the BYLP-D functional and the corresponding dashed curves in the same color are for the BYLP functional.

Figure 9. (a) Frequency distributions of axial, equatorial, full solvation shell and bulk OD modes, (b) Frequency time correlation functions of OD fluctuating frequencies of water molecules in the solvation shell and bulk regions. The solid curves are for the BYLP-D functional and the corresponding dashed curves in the same color are for the BYLP functional.

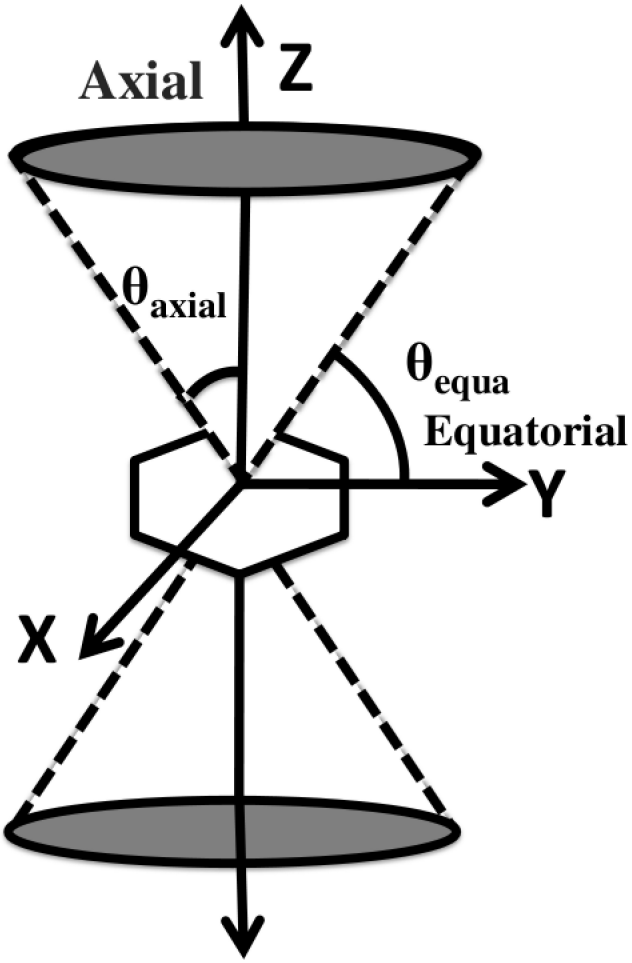

Fig.1

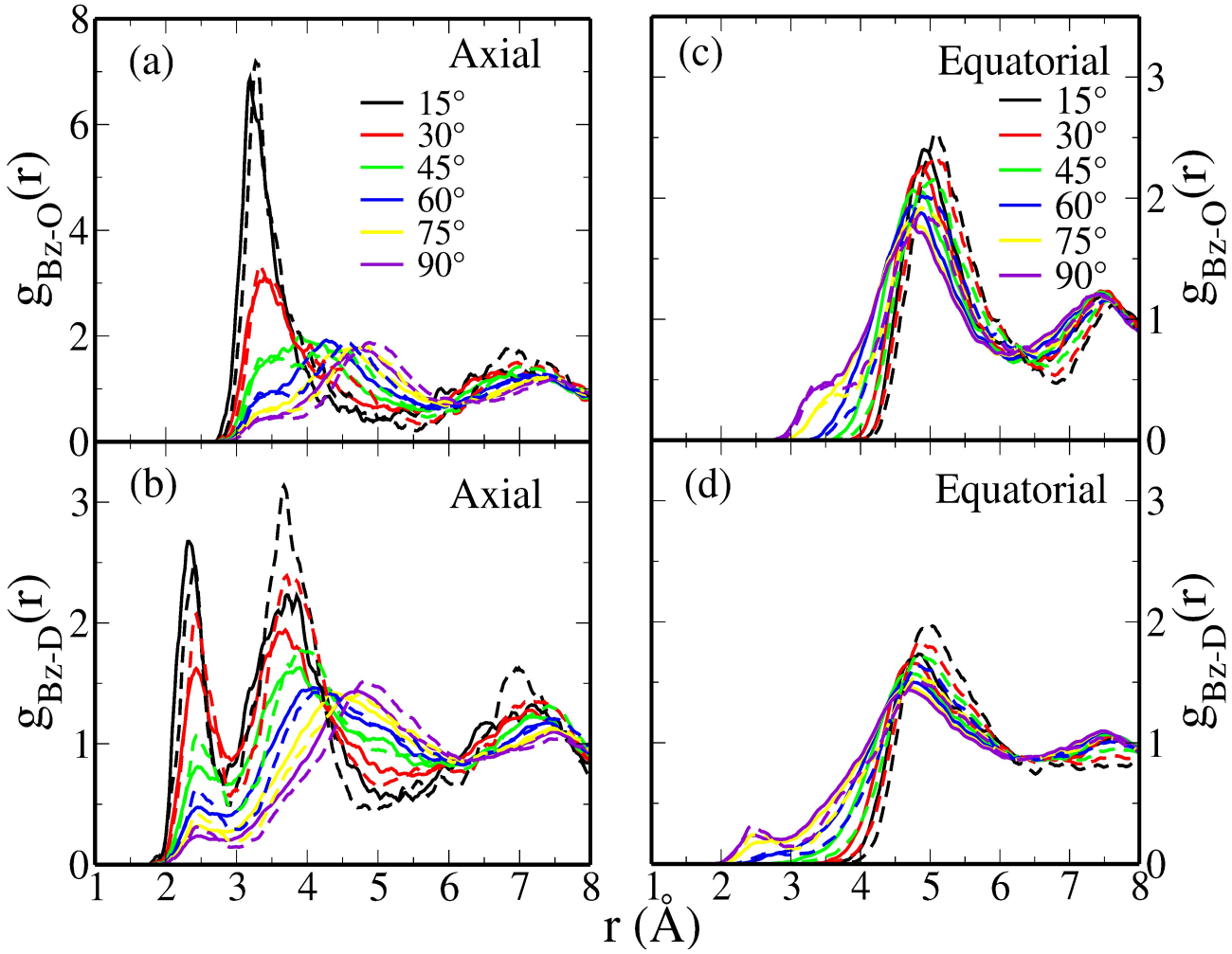

Fig.2

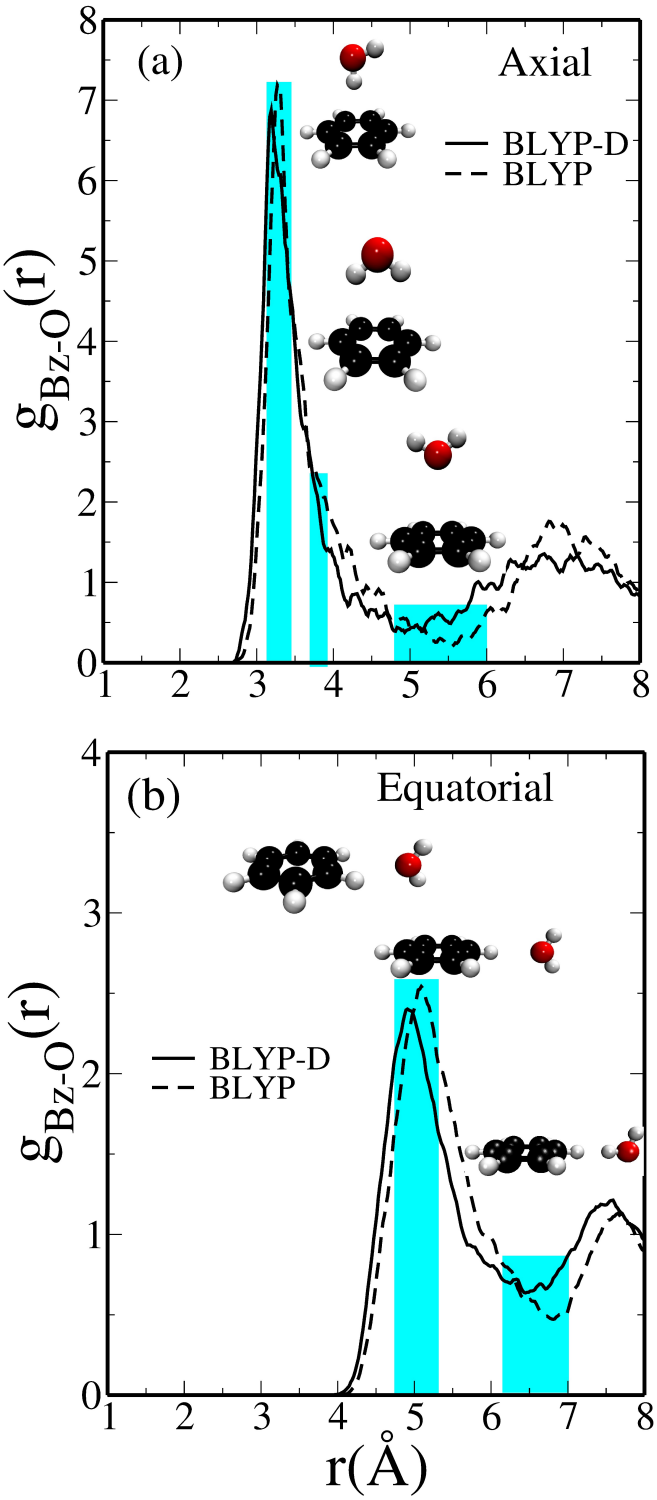

Fig.3

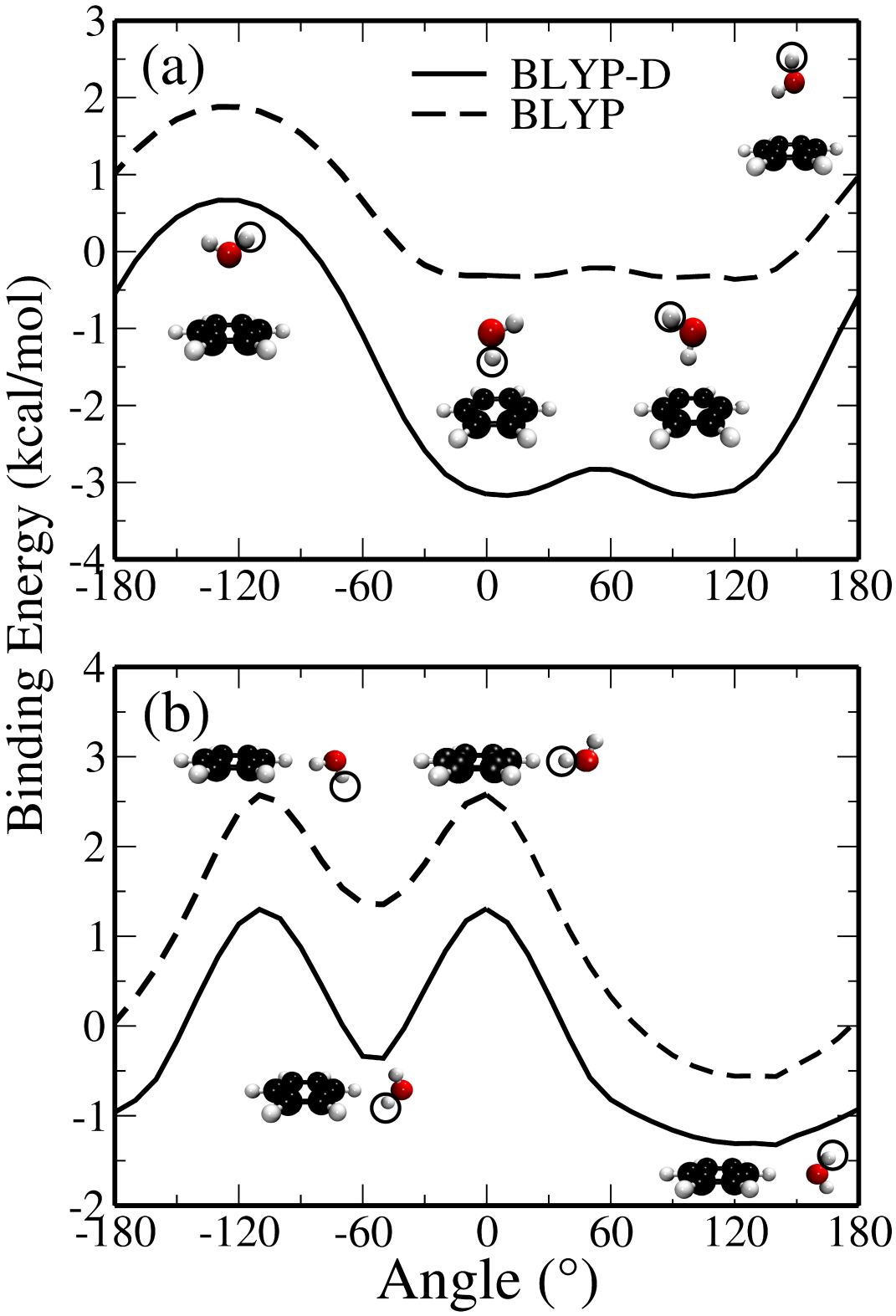

Fig.4

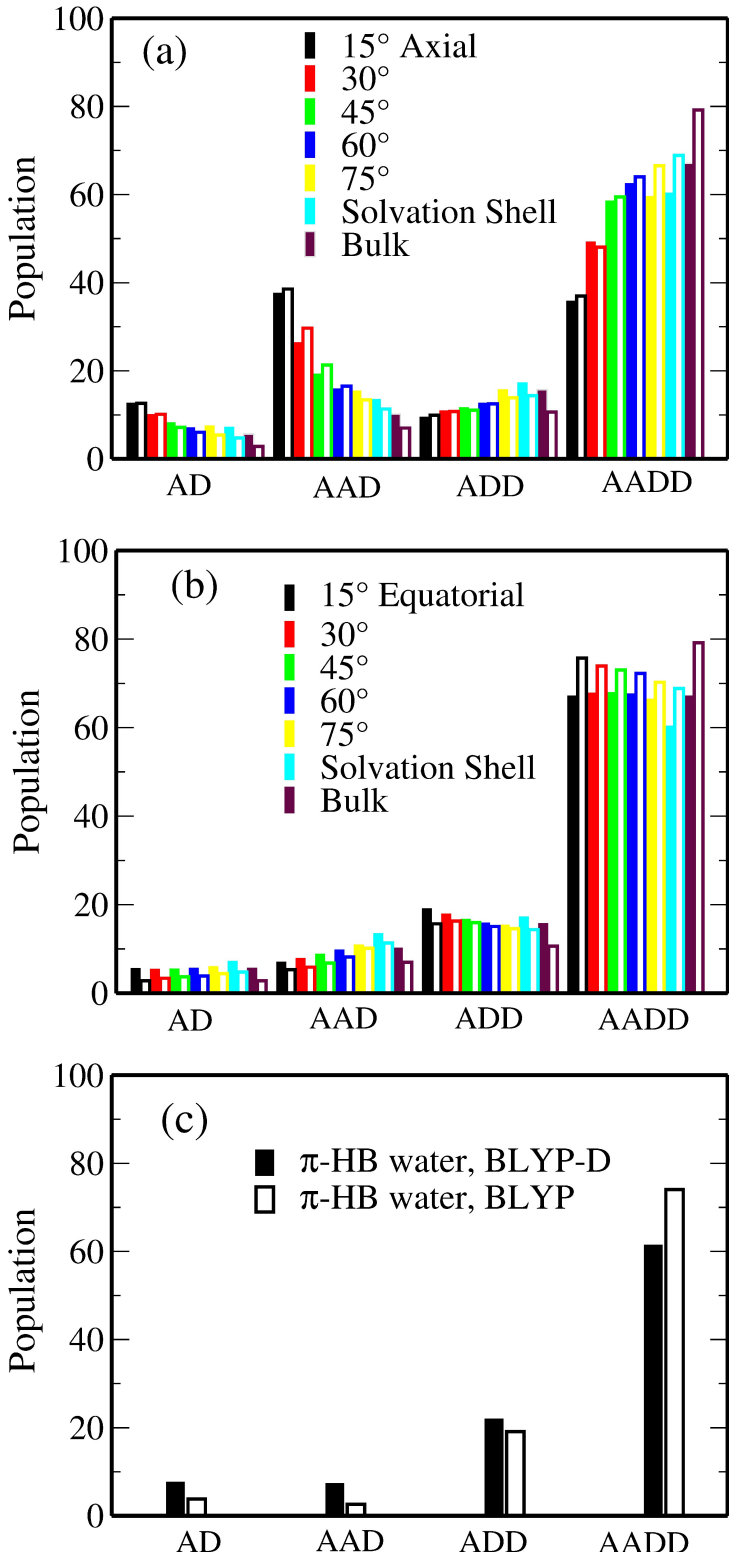

Fig.5

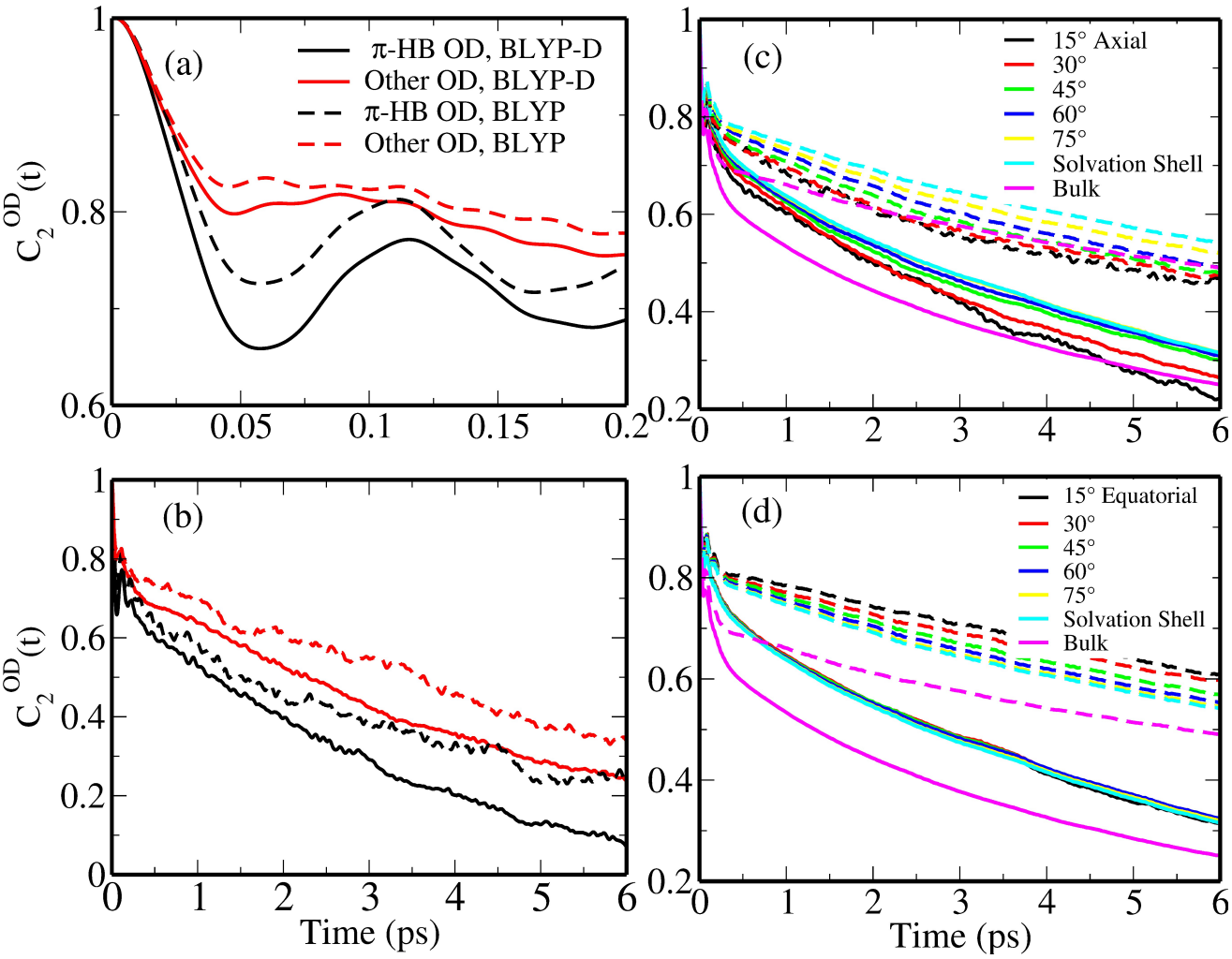

Fig.6

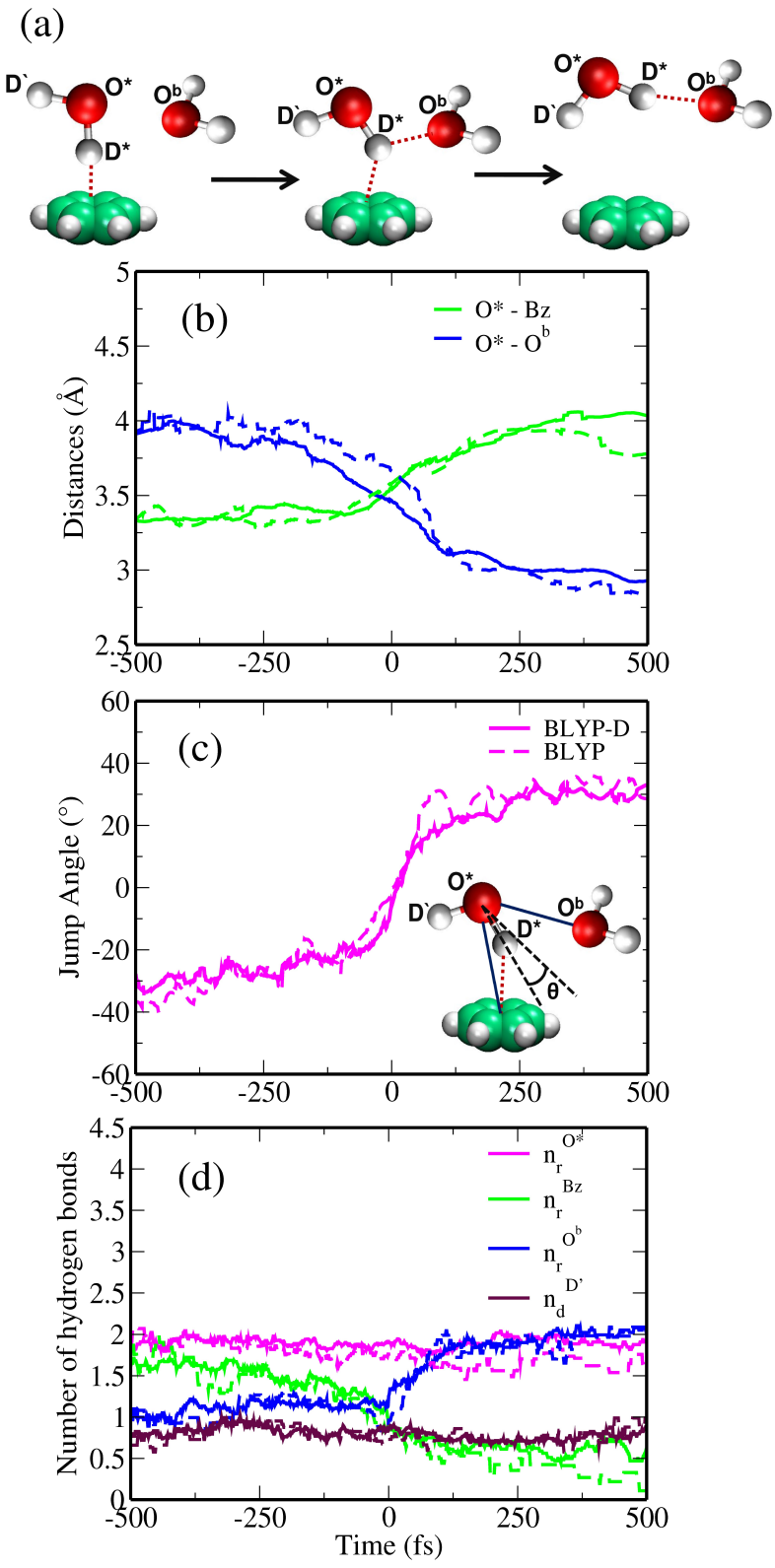

Fig.7

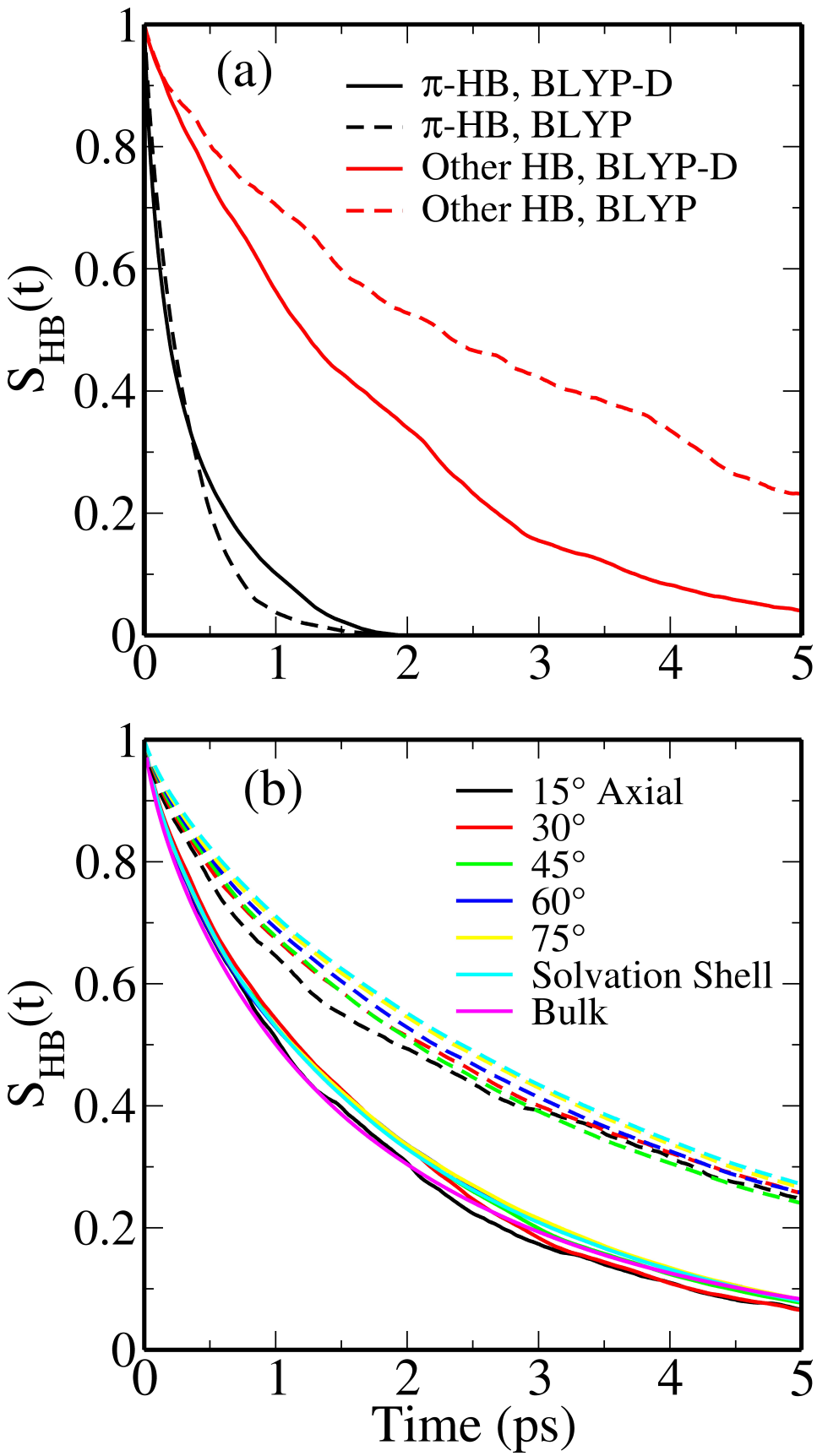

Fig.8

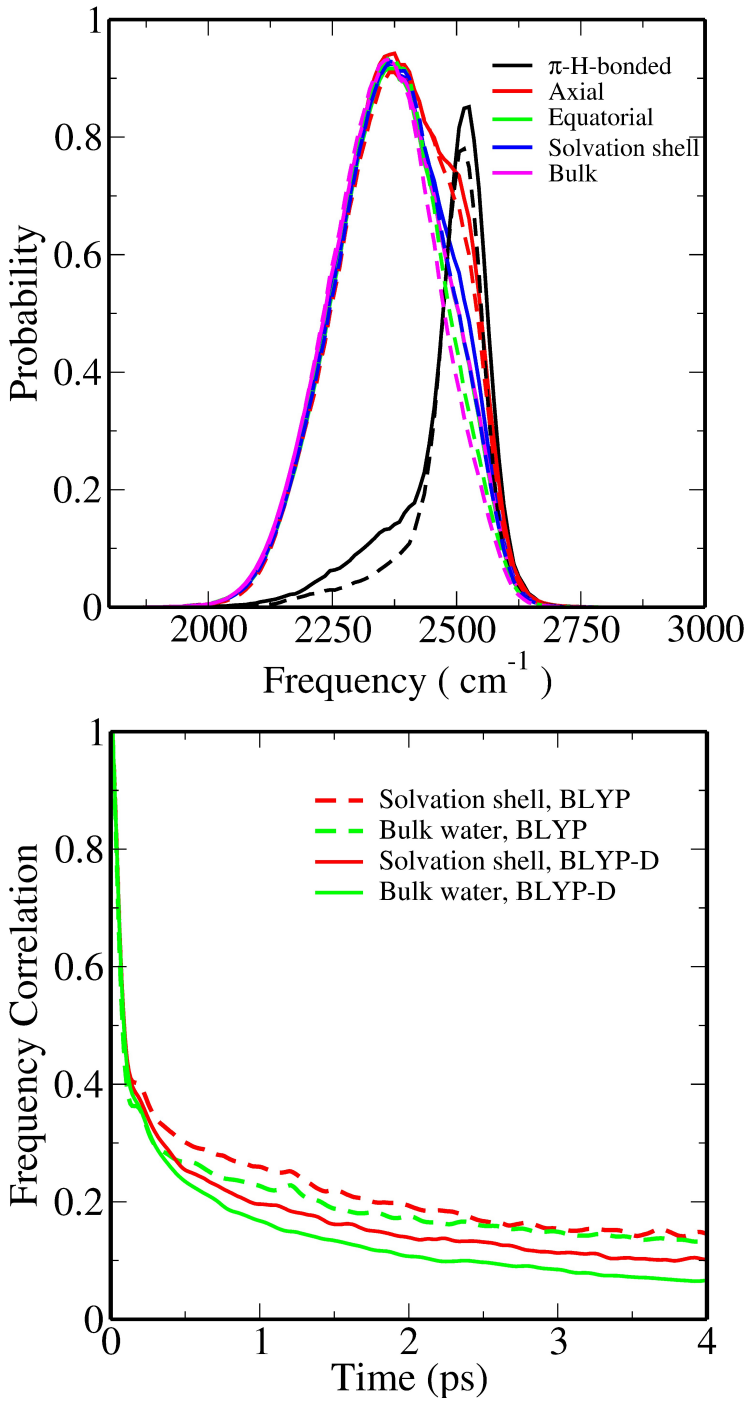

Fig.9

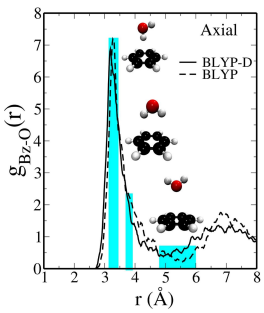

Fig.toc